Article

Not peer-reviewed version

Preparation and Electrochemical Properties of Porous NiCo2O4 Nanostructured Materials by In-Situ Polymerizing Template Method

Chunyang Li , Changsheng An , Guojun Li *

Posted Date: 23 December 2025

doi: 10.20944/preprints202512.1967.v1

Keywords: $NiCo_2O_4$; porous nanostructures; electrochemical properties; polymerizing template method; supercapacitor

 doi:10.20944/preprints202512.1967.v1

Article

Preparation and Electrochemical Properties of Porous $NiCo_2O_4$ Nanostructured Materials by In-Situ Polymerizing Template Method

Chunyang Li [1], Changsheng An [2] and Guojun Li [1,*]

[1] Metal-oxygen New Energy Batteries Key Laboratory of Liaoning Province, Dalian Jiaotong University, Dalian 116028, China

[2] Hunan Key Laboratory of Applied Environmental photocatalysis, Changsha University, Changsha 410022, China

* Correspondence: ligj@djtu.edu.cn

Highlights

- Porous $NiCo_2O_4$ nanomaterials were prepared by using in-situ synthesized template method.
- Porous $NiCo_2O_4$ exhibits 3D macroporous/mesoporous structure.
- Porous $NiCo_2O_4$ nanomaterials are advantageous for increasing cycle life and good rate performance.

Abstract

Porous $NiCo_2O_4$ nanomaterials were prepared by using in-situ synthesized polyacrylamide as template, and cobalt nitrate, nickel nitrate and urea as raw materials. XRD and FESEM results show the spinel type $NiCo_2O_4$ electrode materials with 3D macroporous/mesoporous structure and an average grain size of about 8.1 nm had been synthesized by calcining the amorphous precursor at 300 °C. The electrochemical results of as-calcined $NiCo_2O_4$ showed that the specific capacitance at 10 A g^{-1} is equivalent to 88.9% of 1 A g^{-1}, indicating good rate characteristics. After 3000 cycles, the specific capacity gradually increases from 275.2 F g^{-1} to 678.4 F g^{-1}, and the capacitance retention rate is up to 246.5%, suggesting excellent cycling stability and capacity retention rate.

Keywords: $NiCo_2O_4$; porous nanostructures; electrochemical properties; polymerizing template method; supercapacitor

1. Introduction

Spinel-type $NiCo_2O_4$ has become a very promising electrode material for pseudocapacitor supercapacitors and lithium-ion battery anode due to its advantages of low toxicity, abundant resources, high theoretical capacity and good redox reversibility. However, it wants to be applied in practice, the conductivity, specific capacitance, rate and cycle stability of $NiCo_2O_4$ must be further improved, especially, rate performance and cycle stability are vital for application. Until now, some effective methods such as porous structure [1–3], composite of materials [4–8] and special morphology nanostructure, including 1D nanowires [9,10], 2D nanosheets [11,12], 3D nanoflowers [13] or nanospheres [14] etc. have been adopted. If the more ideal results are got, the combination of two or more methods is necessary [15–17]. In these methods, the porosity can significantly enhance the cycle stability and service life of the electrode materials during the charge and discharge. In general, there are mainly two methods for the synthesis of porous $NiCo_2O_4$ materials. The first, template method [4,11,18,19] is that the macroporous $NiCo_2O_4$ nano-sized electrode materials with one-dimensional (1D), 2D and 3D special morphology are synthesized by hydrothermal method and using conductive foam nickel and carbon cloth as templates. The synthesized materials have high specific capacitance and good rate performance, but the specific capacitance is obviously attenuated

 doi:10.20944/preprints202512.1967.v1

during the charge-discharge cycle. The second, grain agglomeration process [20–22] is that mesoporous $NiCo_2O_4$ nano-sized electrode materials prepared by spray drying method and wet chemical methods combined with calcination process, and the mesopores are formed by the agglomeration and accumulation of nanocrystals during calcinations. And then, the obtained materials have good rate performance and excellent cycle stability, but specific capacitance is relatively low. While maintaining cycle stability and rate performance, the specific capacitance is increased as much as possible, in this paper, a novel in-situ polymerizing template method is employed to the macroporous/mesoporous $NiCo_2O_4$ nanostructured electrode materials. The synthesized material was characterized and its electrochemical properties were studied.

2. Experimental

2.1. Preparation of the Sample

First of all, acrylamide (AM) used as monomer and N, N-methylene diacrylamide (MBAM) used as crosslinker in weight ratio of 19:1 were dissolved in deionized water to prepare a mixed solution with an acrylamide concentration of 7.5 wt%. And then cobalt nitrate, nickel nitrate and urea in the stoichiometric ratio of 2:1:4 were dissolved by using the above mixed solution to obtain 100 mL solution with a 0.3M metal ion concentration. Under constant stirring, 0.2 g of newly prepared 10% ammonium persulfate and ammonium sulfite which performed as initiators was added in the solution drop by drop successively. After initiators were added, the solution was quickly transferred to a sealable container. After standing for 20 min, the polyacrylamide wet gel with 3D network was obtained by in-situ polymerization. The sealed container was put into a 105 °C oven for 6 h to make cobalt nitrate, nickel nitrate and urea react in 3D network. The obtained wet gel was taken out and put it in a 100 °C oven for 24 h to obtain the dried gel precursor. The dried gel precursor is calcined in air at 300 °C for 2 h to produce a black and fluffy sample. In order to remove sulfate ions and other soluble substances, the calcined sample was washed with deionized water until no white precipitate was observed after the filtrate was tested with 0.1M barium acetate solution. The final sample was obtained after the washed sample was dried in a 100 °C oven for 12 h.

2.2. Material Characterization

X-ray diffractometer (XRD, Empyrean with Cu-Kα radiation) and feild emission scanning electron microscope (FESEM, SUPRA 55) were used to study the phase structure and morphology of the sample, respectively. N2 adsorption and desorption test (BET, Quantachrome 3SI-MP-11) method was employed to determine surface area and pore size of the sample. X-ray photoelectron spectroscopy (XPS, PHI 5700) was used to analyze the surface element content of the sample.

2.3. Electrochemical Measurements

The working electrode was prepared by mixing and dispersing 80 wt% the synthesized $NiCo_2O_4$, 10 wt% acetylene black and 10 wt% polyvinylidene fluoride (PVDF) in 1-methyl-2-pyrrolidone (NMP). The mixed slurry was coated on 1 cm^2 of cleaned foamed nickel and dried in vacuum at 110 °C for over 12 h. The mass of the active substance on the electrode was approximately 1 mg. In the three-electrode electrochemical tests at the electrochemical workstation (CHI600B, Shanghai, China), a Hg/HgO was used as reference electrodes, a platinum electrode was used as the counter electrode, and 2M KOH was used as electrolyte.

 doi:10.20944/preprints202512.1967.v1

3. Results and Discussion

3.1. Characterization of as-Calcined $NiCo_2O_4$

Figure 1 is the XRD pattern of the precursor and as-calcined $NiCo_2O_4$. It can be seen from the Figure 1 that no diffraction peak can be observed in the precursor, indicating that the precursor is amorphous. The diffraction peaks of the calcined $NiCo_2O_4$ spectrum are found at 2θ of 31.4 °, 36.75 °, 44.66 °, 59.06 ° and 65.01 °, etc. which are corresponding to (220), (311), (400), (511) and (440) crystal faces of the standard card JCPDS No.73-1702 spinel-type $NiCo_2O_4$, respectively, indicating that spinel-type $NiCo_2O_4$ had been synthesized at 300 °C. In addition, the diffraction peak has obvious broadening effect, suggesting that the particles are very fine.

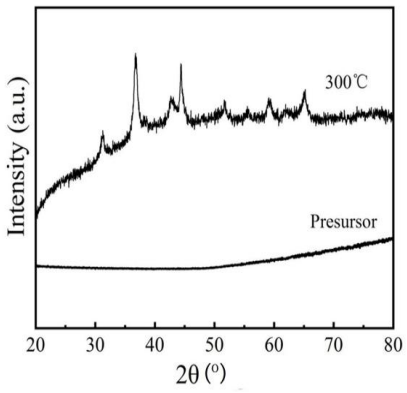

Figure 1. XRD pattern of the precursor and as-calcined $NiCo_2O_4$.

Figure 2 is FESEM images of as-calcined $NiCo_2O_4$. It can be seen from the images that the $NiCo_2O_4$ exhibits a porous structure, most of the pores are smaller than 200 nm in size, and a few can reach 1μm. The formation of macropores is caused by the thermal decomposition and expansion of the in-situ synthesized polyacrylamide polymer with 3D network and the produced inorganic compounds during the calcination.

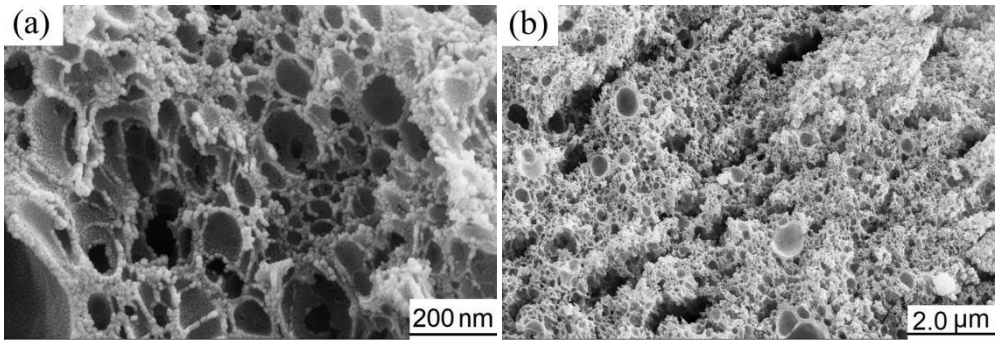

Figure 2. FESEM images of as-calcined $NiCo_2O_4$. (a) 50K X (b) 10K X.

In order to better understand the pore wall, TEM was used to observe the pore wall microstructure of as-calcined samples. Figure 3 is the TEM and SAED images of as-calcined $NiCo_2O_4$. It can be seen from Figure 3a that the pore wall is very thin, that is, the thickness of a nanocrystalline grain. The relatively thick black strips contribute to the molecular chains of the polymer network. The grain size (Figure 3b) has a narrow distribution, ~8.1 nm, and the narrowly distributed nano-sized pores are observed on the grain boundaries. These indicate that the 3D polymer network structure is beneficial to restrain abnormal grain growth and obtain uniform grain size. HRTEM (Figure 3c) and SAED (Figure 3d) shows that $NiCo_2O_4$ is polycrystalline, the interplanar crystal spacing and the index in the space group Fd-3m given by Digital Micrograph software are basically

 doi:10.20944/preprints202512.1967.v1

the same as the corresponding data of spinel $NiCo_2O_4$ (JCPDS card No.20-0781). These characterizations further confirm that the synthesized powder is spinel-type $NiCo_2O_4$.

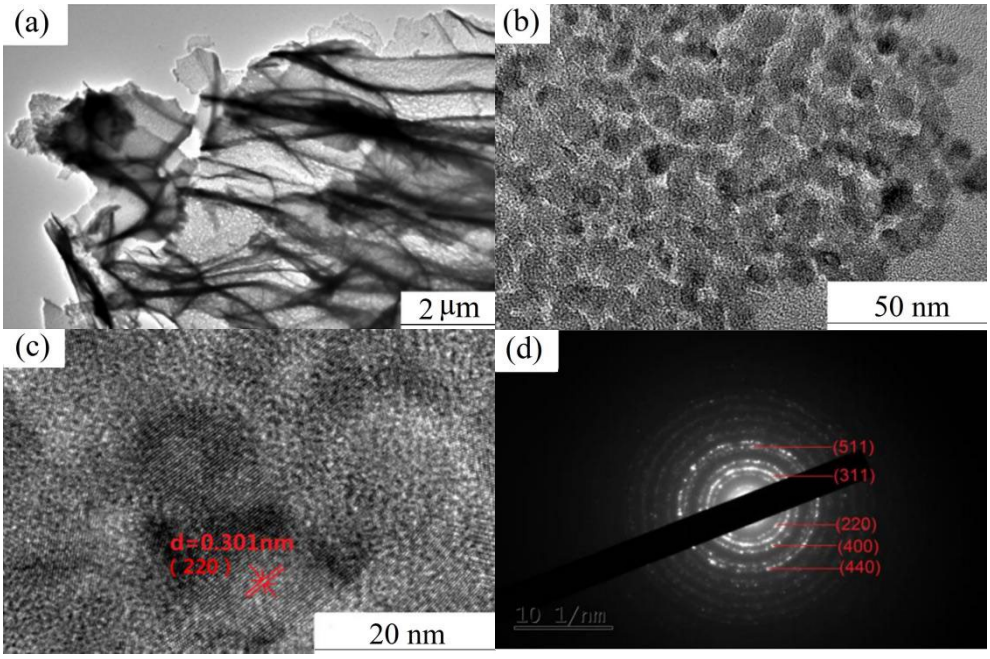

Figure 3. TEM and SAED images of as-calcined $NiCo_2O_4$. (a) and (b) TEM images with different magnifications. (c) HRTEM. (d) SAED image.

Figure 4 shows the test results of N_2 adsorption and desorption. Figure 4a is a typical type IV according to the shape of the curve. P/P0 has obvious hysteresis loop in the range of 0.4 to 1.0, indicating the presence of mesopores. It can be seen from Barrett-Joiner-Halenda (Figure 4b) that the pore size is small, about 3.74 nm and exhibits narrow distribution, which is attributed to the structure of pore wall. The specific surface area of the sample is 76.84 $m^2 g^{-1}$, indicating grain size of as-calcined $NiCo_2O_4$ is very small. These are favorable for the transfer of charge and electrolyte.

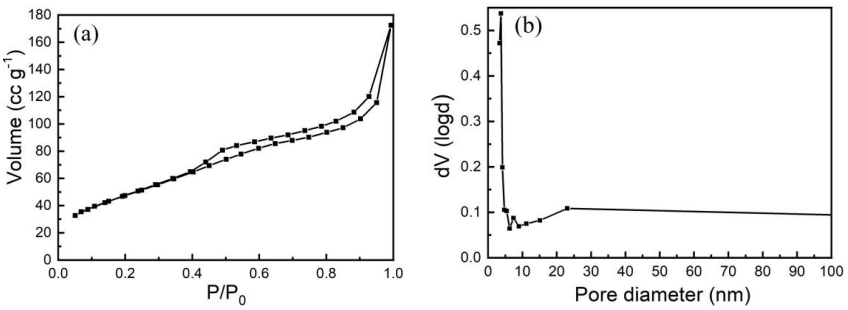

Figure 4. N2 adsorption and desorption isotherms of the calcined sample. (a) BET (b) BJH.

In order to further characterize the element composition and oxidation state of $NiCo_2O_4$, the sample was studied by XPS, and its spectra were shown in Figure 5. The survey spectrum (Figure 5a) indicates the presence of Ni, Co, and O, as well as C from the reference and the absence of other impurities. The XPS core level spectra of the sample were fitted by Gauss-Lorentz method. The Ni 2p emission spectrum (Figure 5b) exhibits two spin-orbit bimodal emission spectra, namely Ni^{2+} and Ni^{3+} and two shake-up satellite peaks (named as "sat."). The binding energies at 854.79 eV and 871.62 eV belong to Ni^{2+}, and the binding energies at 855.55 eV and 873.35 eV belong to Ni^{3+} [23,24]. The emission spectrum of Co 2p (Figure 5c) is consistent with the two characteristic peaks of spin orbit of Co 2p3/2 (779.80 eV) and Co2p1/2 (795.05 eV) and two shake-up satellite peaks (Sat.). The emission peaks at 781.10 eV and 796.80 eV are derived from Co^{2+} [1,26] and the binding energies at 779.70 eV and 794.90 eV are attributed to Co^{3+} [1,26]. There are three oxygen-supplying groups in the O 1s

 doi:10.20944/preprints202512.1967.v1

emission spectra (Figure 5d). O 1 (529.54 eV) is a typical metal-oxygen bond, O 2 (531.8 eV) corresponds to a defect site of low oxygen-coordinated in small-sized particle material, and O 3 (532.2 eV) may be a variety of physically and chemically adsorbed water on and within surface [27]. These results show that the chemical composition of porous $NiCo_2O_4$ nano-structured materials contain Co^{2+} , Co^{3+} , Ni^{2+} , and Ni^{3+} , which are in good agreement with the results in the literature for $NiCo_2O_4$ [1,28].

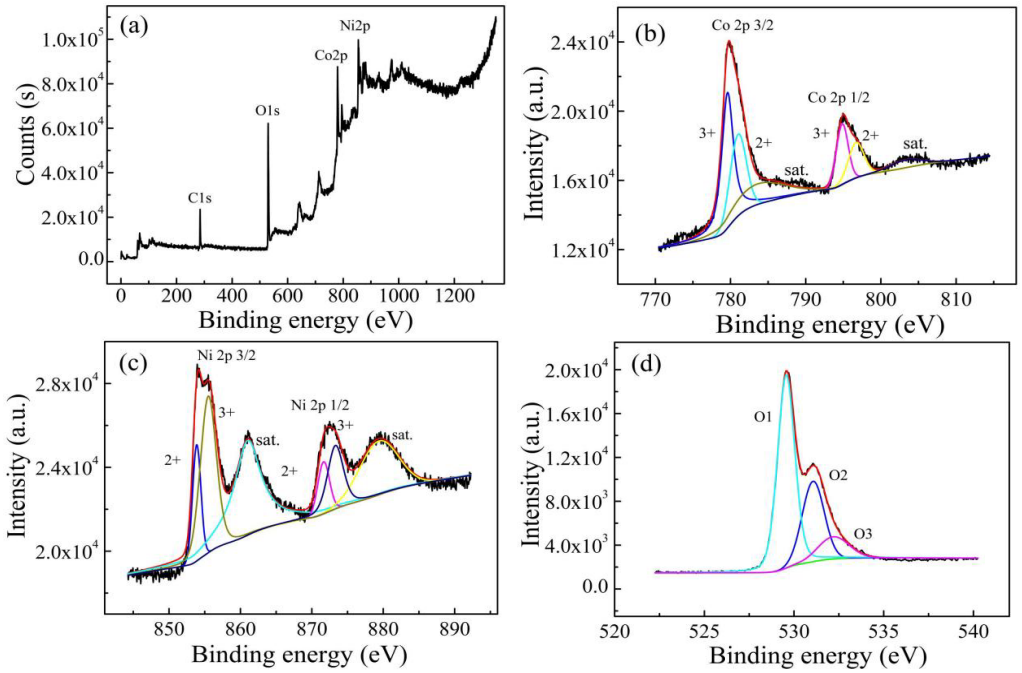

Figure 5. XPS of the $NiCo_2O_4$ microspheres (a) XPS spectrum. (b) Ni 2p (c) Co 2p (d) O 1s.

3.2. Electrochemical Properties

Figure 6 shows the electrochemical performance of as-calcined $NiCo_2O_4$. Figure 6a is the cyclic voltammetry (CV) characteristic curves at different scanning rates. Compared with the approximately rectangular CV curve of double-layer capacitance [1], the CV curve of porous $NiCo_2O_4$ nano-electrode material is a typical pseudocapacitance behavior. In the voltage range of 0-0.6 V (vs HgO/Hg), there is a pair of symmetric redox peaks on each curve, which indicates that charge storage is achieved by the Faradic redox reaction of Co^{2+}/Co^{3+} and Ni^{2+}/Ni^{3+}, and the reaction is reversible. Equations (1) and (2) [29,30] can be used for redox reactions:

$$NiCo_2O_4 + OH^- + H_2O \leftrightarrow NiOOH + 2CoOOH + 2e- \quad (1)$$

$$CoOOH + OH^- \leftrightarrow CoO_2 + H_2O + e- \quad (2)$$

CV curves indicates that the area of the CV curve increases with the increase of the scanning rate, and the positions of the oxidation peak and reduction peak move to the right and left, respectively. The oxidation peak increases from ~ 0.35 V to ~ 0.5 V, and the reduction peaks decrease from ~1.8 V to ~ 0.13 V. When the scanning rate increases, the peak voltage difference increases, indicating that there is polarization in the electrode. the shape of the curves remains relatively better, indicating that the electrode material has good structural stability and cycling stability.

Figure 6b shows the galvanostatic charge-discharge (GCD) curves of porous $NiCo_2O_4$ nano-electrode materials at different current densities in the voltage range of 0-0.5 V. The specific capacitance was calculated by the following equation (3).

$$Cs = I\Delta t/m\Delta V \quad (3)$$

Where CS (F g^{-1}) refers to the specific capacitance, I (A) refers to the discharge current, Δt (s) refers to the discharge time, ΔV (V) refers to a potential change during discharge and m (g) refers to the mass of active material. The specific capacitances at current densities of 1, 2, 4, 6, 8 and 10 A g^{-1} are 371.2, 362.5, 356, 358.67, 344.4, 340.8 and 330.0 F g^{-1}, respectively. As the current density increases,

 doi:10.20944/preprints202512.1967.v1

the specific capacitance decreases. When the current density is 10 A g^{-1}, the specific capacitance is equivalent to 88.9 % of the initial capacitance, indicating high specific capacitance and good rate characteristics of as-synthesized materials. The electrochemical impedance spectra (EIS) of the nano-structured porous $NiCo_2O_4$ and fitting plot of the equivalent circuit are shown in Figure 6c. As observed, the equivalent circuit consists of R_s, R_{ct}, Z_W, C_{dl} and CPE_{PC} [31]. R_s represents the mass transfer resistance and contact resistance, which is reflected by the intercept of the curve and the real axis in high frequency regions [32,33]. R_{ct} refers to the charge transfer resistance caused by the Faradiac reactions, which is reflected by the diameter of the semicircle in the medium-to-high frequency region. Representing the OH^- ions diffusion resistance inside the active material particles, Warburg impedance Z_W is reflected by the oblique line in low frequency region. C_{dl} refers to electric double layer capacitance on the electrode materials [32] and CPE_{PC} represents constant phase element. By contrast with the results in the literatures [33,34], the obtained sample with R_{ct} value of 0.65 Ω is lower or similar, which is advantage for the rapid transfer of charge. The large slope of the oblique line contributes to the OH^- ions rapid diffusion coefficient. The rapid transfer of charge and ions are related to the abundant macroporous/mesoporous structure and small resistance caused by ultra-fine grains small resistance. Thus, the synthesized porous $NiCo_2O_4$ nano-sized material has the better electrochemical reversibility.

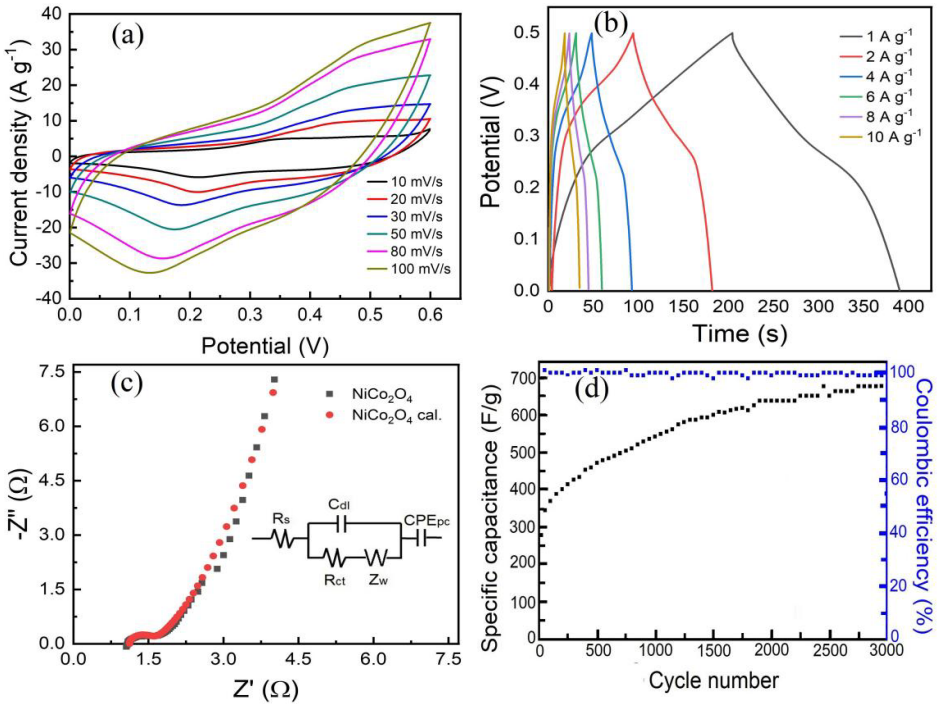

Figure 6. Electrochemical properties of as-calcined $NiCo_2O_4$. (a) CV curves at different scan rates, (b) GCD curves at different current densities, (c) EIS curve and (d) Cycle life and coulomb efficiency of as-calcined $NiCo_2O_4$ nanomaterial at 10 A g^{-1}.

For supercapacitors, the change of capacitance during long time operation at a large current density is an important electrochemical performance parameter for their practical application. Figure 6d shows the cycle life and coulomb efficiency curves of porous $NiCo_2O_4$ nano-siezed electrode materials at a current density of 10 A g^{-1}. The specific capacitance increases with increasing cycle numbers. After 3000 cycles, the specific capacity gradually increases from 275.2 F g^{-1} to 678.4 F g^{-1}, and the capacitance retention rate is excellent, reaching 246.5%. In the first 1000 cycles, the specific capacity increases rapidly, which is generally believed to be related to the activation of the electrode material, because the continuous charging and discharging process activates more contact points, so that the specific capacitance has a significant increase. After 1500 cycles, the specific capacitance increases slowly and becomes stable gradually. It can also be seen that the coulomb efficiency is more

 doi:10.20944/preprints202512.1967.v1

than 99%, which indicates that the obtained material has good electrochemical reversibility, a long and stable cycle life, and relatively stable structure during the charge discharge process.

4. Conclusions

The macroporous/mesoporous $NiCo_2O_4$ nano-electrode materials were successfully synthesized by in-situ polymerizing template method at the calcination of 300 °C. Most of the 3D macropore size is less than 200 nm, mesopore size located on pore walls is about 4nm, and the average grain size is about 8.1 nm. The electrochemical performance of the as-calcined $NiCo_2O_4$ shows that the porous $NiCo_2O_4$ nano-electrode materials have good rate performance (specific capacitance at 10 A g^{-1} equivalent to 88.9% of 1 A g^{-1}), excellent cycle stability at high current density, and long cycle capacity retention (after 3000 cycles, equivalent to 246.5% of the initial capacity). The good rate performance and coulomb efficiency of charge and discharge, long cycle life and capacity retention rate are attributed to the large specific surface area which increases the reaction points of the active substance, the rich macroporous/mesoporous channel structure that is conducive to reduce the charge transfer resistance and plays a buffer to the lattice stress caused by volume change in the process of charge and discharge.

Author Contributions: Conceptualization, C.L. and G.L.; methodology, C.L.; validation, W.L., Y.D. and C.A.; formal analysis, C.L.; investigation, W.L. and Y.D.; data curation, C.L.; writing—original draft preparation, C.L.; writing—review and editing, C.A. and G.L.; supervision, G.L.; project administration, C.L. All authors have reviewed and agreed to the published version of the manuscript.

Funding: This research was funded by Hunan Key Laboratory of Applied Environmental Photocatalysis and Sichuan key Laboratory of Material Corrosion and Protection, grant number 2214503 and 2024CL15, respectively.

Data Availability Statement: Data is available from the corresponding author upon reasonable request.

Acknowledgments: The work was financially supported by Open Fund of Hunan Key Laboratory of Applied Environmental Photocatalysis (No.2214503) and Open Fund of Sichuan key Laboratory of Material Corrosion and Protection (No. 2024CL15).

Conflicts of Interest: The authors declare no conflicts of interest.

References

1. Shen, L.; Che, Q.; Li, H.; Zhang, X. Mesoporous $NiCo_2O_4$ nanowire arrays grown on carbon textiles as binder-free flexible electrodes for energy storage. *Adv Funct Mater* **2014**, *Volume* 24, pp. 2630–2637.
2. Wang, T.; Guo, Y.; Zhao, B.; Yu, S. $NiCo_2O_4$ nanosheets in-situ grown on three dimensional porous Ni film current collectors as integrated electrodes for high-performance supercapacitors. *J Power Sources* **2015,** *Volume* 286, pp. 371-379.
3. Tang, X.; Ren, Q.;Yu, F.D.; Wang, Z.B. The improved cycling stability of nanostructured $NiCo_2O_4$ anodes for lithium and sodium ion batteries. *Ionics* **2023**, *Volume* 29, pp. 3943–3954.
4. Yang, F.; Zhang, K.; Li, W.; Xu, K. Structure-designed synthesis of hierarchical $NiCo_2O_4$@NiO composites for high-performance supercapacitors. *J Colloid & Interface Sci* **2019,** *Volume* 556, pp. 386–391.
5. Chen, D.; Pang, D.; Zhang, S.; Song, H.; Zhu, W.; Zhu, J. Synergistic coupling of $NiCo_2O_4$ nanorods onto porous Co_3O_4 nanosheet surface for tri-functional glucose, hydrogen-peroxide sensors and supercapacitor. *Electrochim Acta* **2020**, *Volume* 330, pp. 135326.
6. Yuan, Y.; Wang, W.; Yang, J.; Tang, H.; Ye, Z.; Zeng, Y.; Lu, J. Three-dimensional $NiCo_2O_4$@$MnMoO_4$ core-shell nanoarrays for high-performance asymmetric supercapacitors. *Langmuir ACS J Surf Colloids* **2017**, *Volume* 33, pp. 10446–10454.
7. Zeng, W.; Wang, L.; Shi, H.; et al. Metal–organic- framework-derived ZnO@C@$NiCo_2O_4$ core–shell structures as an advanced electrode for high-performance supercapacitors. *J Mater Chem A* **2016**, *Volume* 4, pp. 8233-8241.

 doi:10.20944/preprints202512.1967.v1

8. Zou, R.; Xu, K.; Wang, T.; He, G.; Liu, Q.; Liu, X. Chain-like $NiCo_2O_4$ nanowires with different exposed reactive planes for high-performance supercapacitors. *J Mater Chem A* **2013**, *Volume* 1, pp. 8560-8566.
9. Jiang, H.; Ma, J.; Li, C. Hierarchical porous $NiCo_2O_4$ nanowires for high-rate supercapacitors. *Chem Commun* **2012**, *Volume* 48, pp. 4465-4467.
10. Yuan, C.; Li, J.; Hou, L.; Zhang, X.; Shen, L.; Lou, X.W. Ultrathin mesoporous $NiCo_2O_4$ nanosheets supported on Ni foam as advanced electrodes for supercapacitors. *Adv Funct Mater* **2012**, *Volume* 22, pp. 4592–4597.
11. Zhang, G.; Lou, X.W. General solution growth of mesoporous $NiCo_2O_4$ nanosheets on various conductive substrates as high-performance electrodes for supercapacitors. *Adv Mater* **2013**, *Volume* 25, pp. 976-979.
12. Karmakar, S.; Varma, S.; Behera, D. Investigation of structural and electrical transport properties of nano-flower shaped $NiCo_2O_4$ supercapacitor electrode materials. *J Alloys & Comp* 2018, *Volume* 757, pp. 49-59.
13. Pang, M.J.; Jiang, S.; Long, G.H.; Ji, Y.; Han, W.; Wang, B. et al. Mesoporous $NiCo_2O_4$ nanospheres with a high specific surface area as electrode materials for high-performance supercapacitors. *RSC Adv* **2016**, *Volume* 6, pp. 67839-67848.
14. Xue, W.; Wang, W.; Fu, Y.; He, D.; Zeng, F.; Zhao, R. Rational synthesis of honeycomb-like $NiCo_2O_4$@$NiMoO_4$ core/shell nanofilm arrays on Ni foam for high-performance supercapacitors. *Mater Lett* **2017**, *Volume* 186, pp.34-37.
15. Sun, S.; Li, S.; Wang, S.; Li, Y.; Wang, P. Fabrication of hollow $NiCo_2O_4$ nanoparticle /graphene composite for supercapacitor electrode. *Mater Lett* **2016**, *Volume* 182, pp. 23-26.
16. Tomboc, G.M.; Kim, H. Derivation of both EDLC and pseudocapacitance characteristics based on synergistic mixture of $NiCo_2O_4$ and hollow carbon nanofiber: An efficient electrode towards high energy density supercapacitor. *Electrochim Acta* 2019, *Volume* 318, pp.392-404.
17. Zhang, D.; Yan, H.; Lu, Y. et al. Hierarchical mesoporous nickel cobaltite nanoneedle/carbon cloth arrays as superior flexible electrodes for supercapacitors. *Nanoscale Res Lett* **2014**, *Volume* 9, pp.139-148.
18. Guo, D.; Zhang, L.; Song, X.; Tan, L. $NiCo_2O_4$ nanosheets grown on interconnected honeycomb-like porous biomass carbon for high performance asymmetric supercapacitor. *New J Chem* **2018**, *Volume* 42, pp. 8478-8484.
19. Li, C.; Liu, Y.; Li, G.; Ren, R. Preparation and electrochemical properties of nanostructured porous spherical $NiCo_2O_4$ materials. *RSC Adv* **2020**, *Volume* 10, pp.9438-9443.
20. Wu, Y.Q.; Chen, X.Y.; Ji, P.T.; Zhou, Q.Q. Sol–gel approach for controllable synthesis and electrochemical properties of $NiCo_2O_4$ crystals as electrode materials for application in supercapacitors. *Electrochim Acta* **2011**, *Volume* 56, pp. 7517-7522.
21. Wu, S.; Liu, Q.; Yan, Q.; Jiang, H.; wang, Q. Synthesis and electrochemical properties of $NiCo_2O_4$ nanoparticles. *J Chin Ceram Soc* **2017**, *Volume* 45, pp. 504-509.
22. Lin, W.C.; Guo, W.G.; Wang, L.H. Synthesis crystal structure and characterization of a new zinc citrate complex. *Chin J Struc Chem* **2014**, *Volume* 33, pp. 591-596.
23. Tang, X.; Ren, Q.; Yu, F.D.; Wang, Z.B. The improved cycling stability of nanostructured $NiCo_2O_4$ anodes for lithium and sodium ion batteries. *Ionics* **2023**, *Volume* 29, pp. 3943-3954.
24. Hao, P.; Tian, J.; Sang, Y. et al. 1D Ni-Co oxide and sulfide nanoarray/carbon aerogel hybrid nanostructures for asymmetric supercapacitors with high energy density and excellent cycling stability. *Nanoscale* **2019**, *Volume* 8, pp. 16292-16301.
25. Lu, X.F.; Wu, D.J.; Li, R.Z.; Li, Q.; Tong, Y.X.; Li, G.R. Hierarchical $NiCo_2O_4$ nanosheets@hollow microrod arrays for high-performance asymmetric supercapacitors. *J Mater Chem A* **2014**, *Volume* 2, pp. 4706-4713.
26. Lei, Y.; Li, J.; Wang, Y.; Gu, L.; Chang, Y.; Yuan, H.; Xiao, D. Rapid microwave-assisted green synthesis of 3D hierarchical flower-shaped $NiCo_2O_4$ microsphere for high-performance supercapacitor. *ACS Appl Mater & Interfaces* **2014**, *Volume* 6, pp. 1773−1780.
27. Li, J.; Xiong, S.; Liu, Y.; Ju, Z.; Qian, Y. High electrochemical performance of monodisperse $NiCo_2O_4$ mesoporous microspheres as an anode material for li-ion batteries. *ACS Appl Mater & Interfaces* **2013**, *Volume* 5, pp. 981-988.
28. Gao, S.; Liao, F.; Ma, S.; Zhu, L.; Shao, M. Network-like mesoporous $NiCo_2O_4$ grown on carbon cloth for high-performance pseudocapacitors. *J Mater Chem* A **2015**, *Volume* 3, pp. 16520-16527.

 doi:10.20944/preprints202512.1967.v1

29. Liu, W.W.; Lu, C.; Liang, K.; Tay, B.K. A three dimensional vertically aligned multiwall carbon nanotube/$NiCo_2O_4$ core/shell structure for novel high-performance supercapacitors. *J Mater Chem A* **2014**, *Volume* 2, pp. 5100-5107.
30. Nwanya, A.C.; Offiah, S.U.; Amaechi, I.C. et al. Electrochromic and electrochemical supercapacitive properties of room temperature PVP capped $Ni(OH)_2$/NiO thin films. *Electrochim Acta* **2015**, *Volume* 171, pp. 128-141.
31. Xie, X.; Chang, Z.; Wu, M.; Tao, Y.; Lv, W.; Yang, Q.H. Porous MnO_2 for use in a high performance supercapacitor: replication of a 3D graphene network as a reactive template. *Chem Commun* **2013**, *Volume* 49, pp. 11092-11094.
32. Cai, D.; Liu, B.; Wang, D. et al. Construction of unique $NiCo_2O_4$ nanowire@$CoMoO_4$ nanoplate core/shell arrays on Ni foam for high areal capacitance supercapacitors. *J Mater Chem A* **2014**, *Volume* 2, pp. 4954-4960.
33. Padmanathan, N.; Selladurai, S. Controlled growth of spinel $NiCo_2O_4$ nanostructures on carbon cloth as a superior electrode for supercapacitors. *RSC Adv* **2014**, *Volume* 4, pp. 8341-8349.